Missing theoretical evidence for conventional room-temperature superconductivity in low-enthalpy structures of carbonaceous sulfur hydrides

Moritz Gubler,[1] José A. Flores-Livas,[2,3] Anton Kozhevnikov,[4] and Stefan Goedecker[1]
[1]*Department of Physics, University of Basel, Klingelbergstrasse 82, CH-4056 Basel, Switzerland*
[2]*Dipartimento di Fisica, Università di Roma La Sapienza, Piazzale Aldo Moro 5, I-00185 Roma, Italy*
[3]*RIKEN Center for Emergent Matter Science, 2-1 Hirosawa, Wako 351-0198, Japan*
[4]*CSCS, Swiss National Supercomputing Centre, Via Trevano 131, CH-6900 Lugano, Switzerland*

(Received 21 September 2021; revised 19 November 2021; accepted 14 December 2021; published 6 January 2022)

To elucidate the geometric structure of the putative room-temperature superconductor, carbonaceous sulfur hydride (C-S-H), at high pressure, we present the results of an extensive computational structure search of bulk C-S-H at 250 GPa. Using the minima hopping structure prediction method coupled to the GPU-accelerated SIRIUS library, more than 17 000 local minima with different stoichiometries in large simulation cells were investigated. Only 24 stoichiometries are favorable against elemental decomposition, and all of them are carbon-doped H_3S crystals. The absence of van Hove singularities or similar peaks in the electronic density of states of more than 3000 candidate phases rules out conventional superconductivity in C-S-H at room temperature.

DOI: 10.1103/PhysRevMaterials.6.014801

I. INTRODUCTION

In late 2020 the group of Dias published evidence for the first room-temperature superconductor (RTS) at 289 K and 267 GPa [1]. According to the authors, the superconductive material is carbonaceous sulfur hydride (C-S-H) produced by photochemical synthesis at high pressure. In their work, the authors initially mixed carbon and sulfur at a 1:1 molar ratio; then, the sample was put into gaseous hydrogen, pressurized in a diamond anvil cell, and exposed to 532 nm laser light, a wavelength known to break sulfur bonds. Unfortunately, despite the relative simplicity of the recipe, no other researchers were able to reproduce this synthesis pathway and the exact stoichiometry and crystalline structure remain unknown.

More recently, Lamichhane *et al.* [2] examined the x-ray diffraction patterns for samples of C-S-H polymorphs and determined their equation of state. They pointed out that the structure could have the composition $[(CH_4)_2]_x[(H_2S)_2H_2]_y$ where y is much bigger than x. However, measurements of resistivity or magnetic response were not carried out to corroborate the superconducting state. Experimentally, the fact that hydrogen is involved with high pressure challenges the accurate determination of the possible crystalline structures.

On the theoretical side, Sun *et al.* [3] and Cui *et al.* [4] published the results of structure searches in the C-S-H ternary before the publication of the results of Dias's group. These theoretical studies focused on pressures of 100 and 200 GPa, lower than the reported pressure for the RTS (close to 270 GPa). However, extrapolating the results from lower to high pressures is unreliable since the chemistry changes drastically with every GPa gained. Nevertheless, not a single candidate was found to be thermodynamically stable among all the structures explored in these works.

A fresher look recently came from Wang and co-workers [5], who studied the 250 GPa domain, and ruled out doping as a possible explanation of the RTS. However, while their crystalline search was thorough, it focused on small doping regions near the known H_3S superconductor.

Moreover, a debate is rising in the literature concerning the uncommon superconducting features of the C-S-H compound [6–10], namely a sharp drop of electric resistivity at T_c and an unusual dependence on magnetic fields [6].

In this paper, we studied the enthalpy landscape of C-S-H at two different pressures thoroughly. Owing to the use of graphical processing units (GPU), we could extend our searches to larger crystalline cells using highly accurate density functional theory (DFT). We organize the rest of the paper as follows: Sec. II provides details on our numerical methodology to calculate *ab initio* the enthalpy landscape and details on the algorithmic searches. Section III presents the results of the thermodynamic phase diagram, a comparison between two DFT functionals, the pressure dependence, and a benchmark against an all-electron basis set. Finally, we search for peaks in the electronic density of states near the Fermi level that could explain the experimental results.

II. METHODS

A. Structure search

The compositional and configurational space of C-S-H was explored at 250 and 300 GPa using the minima hopping method [11–14]. Minima hopping is an efficient method to find low-energy minima on the potential energy surface. In contrast to numerous other algorithms such as simulated annealing [15] or basin hopping [16] it is not based on thermodynamic principles. The method uses a combination of

molecular dynamics and geometry optimizations to explore the entire configuration space without visiting known parts of it many times.

Three different sections of compositions in the ternary phase diagram were selected based on the following: (I) experimental input (central region), (II) high-hydrogen content regions that make it more likely to find a high-temperature superconductor, and (III) the region designed as "doping" for its similarity to the H_3S phase.

We first scrutinized the 250 GPa pressure range extensively and examined the 300 GPa region afterwards. We invested the bigger part of our resources in the search at 250 GPa since this pressure range is reported most promising [1].

The GPU-accelerated SIRIUS [17] library was used to calculate energy, atomic forces, and stresses at the DFT level with the local density approximation (LDA) exchange-correlation functional and ultrasoft pseudopotentials [18]. A plane-wave basis set with a cutoff energy of 300 eV was used to expand the wave function. Geometry relaxations were performed with tight convergence criteria such that the forces on the atoms and the lattice derivatives were less than 5 meV/Å.

B. Postprocessing with all-electron calculations

Out of the more than 17 000 structures, 3000 were further studied. All structures that have an enthalpy close to the putative ground state (less than 20 meV per atom) of each stoichiometry were selected for further analysis. This means that even thermodynamically unstable structures and stoichiometries were thoroughly investigated for high critical temperatures.

To eliminate possible inaccuracies from the pseudopotential at these high pressures, the selected systems were further analyzed with the all-electron FHI-AIMS code using the more accurate Perdew-Burke-Ernzerhof (PBE) functional [19]. A full geometry relaxation (lattice vectors and atomic positions) was carried out with the tier 2 basis set of FHI-AIMS. Afterwards, the density of states was calculated and inspected for all these 3000 structures. We looked for narrow peaks in the electronic density of states (DOS) at the Fermi level, a necessary feature for conventional high T_c (HTC) superconductors [20–23]. Systems with promising peaks at the Fermi level were analyzed even further and their T_c was calculated. This is process is described in the next section.

C. Calculation of electron-phonon interaction coefficients

Structures with peaks at the Fermi level in the density of states and that do not lie in the doping region pictured in Fig. 1 were selected for further analysis. Using QUANTUM ESPRESSO [24] the electron-phonon interaction coefficient λ was calculated and the critical temperature was obtained with the Allen-Dynes equation [25]. The doping region was excluded because Wang *et al.* [5] already calculated the transition temperature for most of the relevant systems in it. It was carefully checked that the electron-phonon interaction was calculated with converged parameters. The calculations were done with an ultrasoft pseudopotential [18], 800 eV as the plane-wave cutoff energy, a $64 \times 64 \times 64$ k grid (a spacing of $\sim$0.04 Å^{-1}) and a $5 \times 5 \times 5$ q grid which corresponds to a spacing of $\sim$0.5 Å^{-1}.

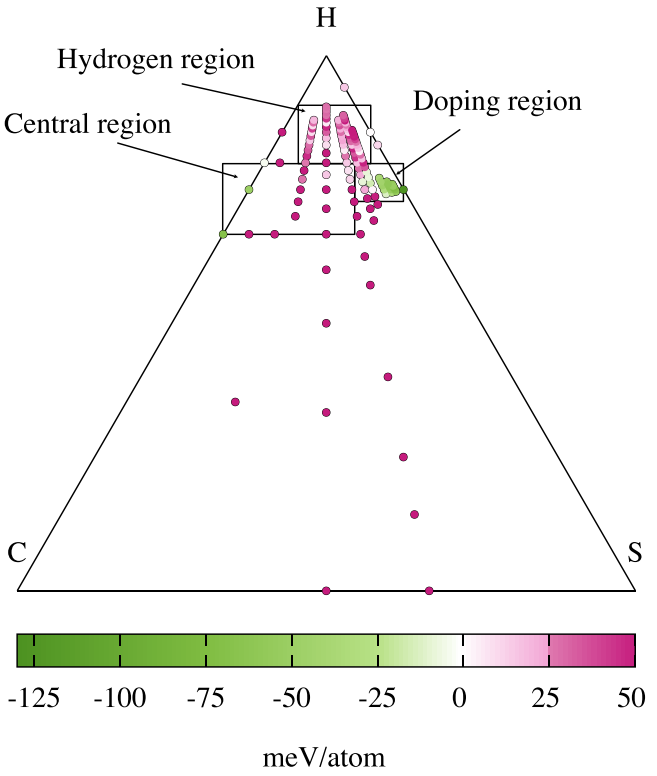

FIG. 1. The ternary convex hull of formation enthalpy generated from 140 stoichiometries explored at 250 GPa. The formation enthalpy per atom can be read off the color bar. In addition we zoom into the three sections of interest that were studied in detail (central, high H, and doping) in Figs. 2, 3, and 4, respectively.

III. RESULTS

The first three sections here discuss our findings at 250 GPa. The last section here is dedicated to the results at 300 GPa.

A. Structures and energies of the ternary phases at 250 GPa

Figure 1 shows the C-S-H ternary convex hull constructed for 140 compositions at 250 GPa. We subdivide it in three sections to improve readability and analyze regions of the phase diagram carefully. The first section is the central region, based on the experiments by Snider *et al.* [1] and Lamichhane *et al.* [2] in which carbon and sulfur were mixed at a 1:1 molar ratio and with a subsequent hydrogen incorporation. The second region is the high-hydrogen content section. The third section is the doping region, close to the H_3S superconductor. The color bar at the bottom of the figure depicts the composition's enthalpy formation in meV/atom.

The absence of a well-defined ground state, whose energy is considerably lower than for related structures, is evident. Despite the use of larger simulation cells and extensive searches that found up to hundreds of structures per stoichiometry, a decisive structural motif is missing in all structures. Let us start the analysis with the central area,

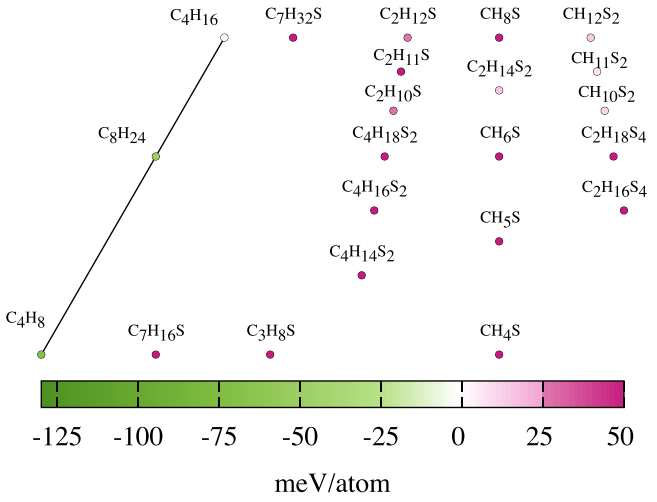

FIG. 2. Center region of the ternary phase diagram at 250 GPa.

depicted in detail in Fig. 2. According to the description of the experiments by Snider *et al.*, the RTS has likely been synthesized in this zone (at least at low pressure). The building blocks of CH_2, CH_3, and CH_4 are found in this region. The saturated carbon bonds lead to semiconducting phases with band gaps between 0.7 and 1.2 eV. The possibility of sulfur doping CH_x can be ruled out accordingly to Ref. [26].

The hydrogen-rich zone, shown in Fig. 3, was extensively reviewed in this work. In this region binaries appear as the lowest enthalpy structures, in this case, CH_4 (−4 meV) followed by H_6S (−1 meV) and H_5S (9 meV). The best ternaries exhibit a slightly higher formation energy. Ternaries with the lowest formation enthalpy are $CH_{10}S$ (8 meV), $CH_{14}S$ (4 meV), $CH_{14}S_2$ (4 meV), and $CH_{23}S_4$ (2 meV).

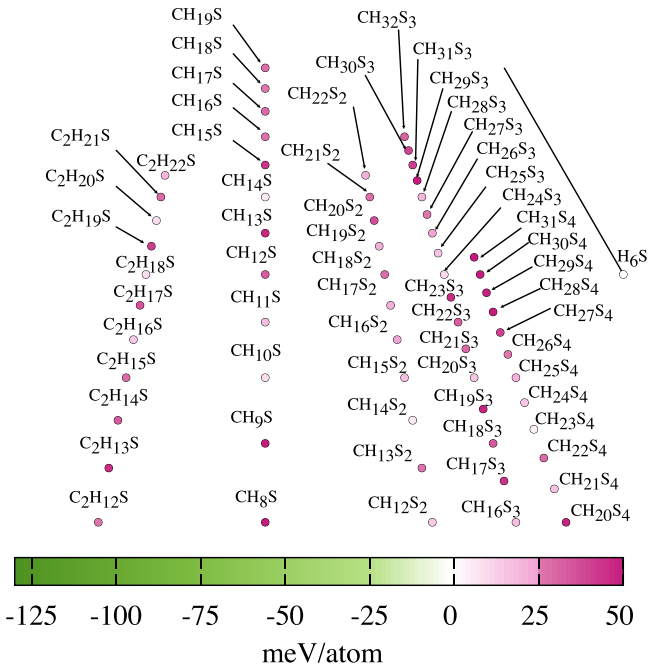

FIG. 3. Hydrogen-rich region of the ternary phase diagram at 250 GPa.

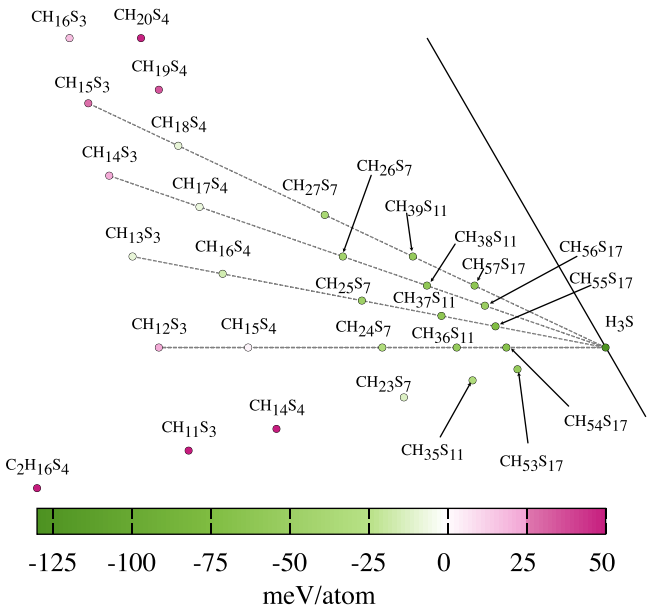

FIG. 4. Carbon doping region of the ternary phase diagram at 250 GPa. The DOS of the structures lying on a gray dashed line are displayed in one of the plots of Fig. 7.

Finally, another region previously reported as promising is the doping area. In this work, we extended the search of the doping area conducted by Wang *et al.* [5] by systematically varying carbon, sulfur, and hydrogen as shown by the dashed lines (slopes) in Fig. 4. The lowest-energy doped system was 5.88% carbon ($CH_{53}S_{17}$). It is noticeable that the formation enthalpy decreases as one approaches the H_3S phase. Also worth mentioning is the sudden jump of enthalpies, suggesting a regime change, going from CH_xS_7 to CH_yS_4. H_3S is the most stable composition at 250 GPa with a formation enthalpy of −130 meV. Its closest neighbors are carbon-doped H_3S crystals which are the ternaries with the lowest formation enthalpy.

We also checked the influence of the exchange-correlation functional in describing the ternary's phase diagram. Figure 5 shows the enthalpy difference between the LDA and generalized gradient approximation (GGA), at 250 GPa, for the lowest configuration for each stoichiometry calculated by FHI-AIMS. Only minor differences are visible in the sulfur and hydrogen areas. Larger deviations start to appear towards the carbon areas of the ternary CH_xS compositions lying on the middle line.

This can be explained by the well-known overbinding of LDA while PBE rather underbinds. The discrepancy between the two functionals is particularly pronounced for solids with molecular building blocks. Metallic systems are described reasonably well with both functionals. This is of course the most important class, since we do not expect that superconductivity arises from a semiconducting or insulating phase.

B. Low-enthalpy compositions

Among all the 140 studied compositions, the doping region appears as the most densely populated one. Other structures having a reasonably low formation enthalpy at 250 GPa are

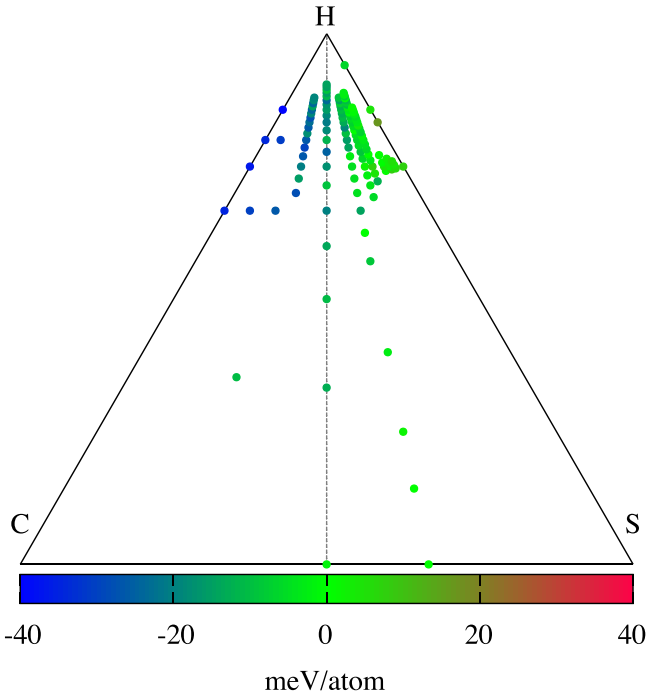

FIG. 5. Comparison of formation enthalpy difference per atom between a PBE and an LDA functional at 250 GPa.

CH_7S, $CH_{10}S_2$, and $CH_{11}S_2$. Figure 6 shows the crystalline structure for these compositions. On the left, the crystal model represents CH_7S, which belongs to the cubic crystal structure, fairly similar to the $Im\bar{3}m$ motif of H_3S. In this structure, every second sulfur atom and the corresponding hydrogen atoms are replaced by a CH_4 molecule. The methane component changes its orientation along the z axis. $CH_{10}S_2$ and $CH_{11}S_2$ (center and right models) in Fig. 6 consist of two layers with an H_3S structure separated by a carbon layer with different hydrogen environments.

C. Electronic density of states

The density of states was calculated and analyzed for the 3000 lowest local minima that were found. A selection of systems with the most promising DOS is discussed here. Figure 7 displays the DOS for most carbon-doped H_3S structures. The lowering of the peak at the Fermi level with a higher carbon concentration indicates inferior superconductive properties compared to H_3S. The peaks in DOS also move away from the Fermi level. In Figs. 7(a) and 7(b) they move to the right, and in Figs. 7(c) and 7(d) they move to the left. This is indicated by the gray dashed lines in Figs. 7(a)–7(d). In the central region of the ternary phase diagram CH_7S, $CH_{10}S_2$ and $CH_{11}S_2$ have a low formation enthalpy and some interesting features in the DOS at the Fermi level displayed in Fig. 6(e). When their peak at the Fermi level is compared to the H_3S superconductor in Fig. 6(e) none of them is as sharp as the one in the H_3S system which indicates a lower critical temperature than the one of H_3S.

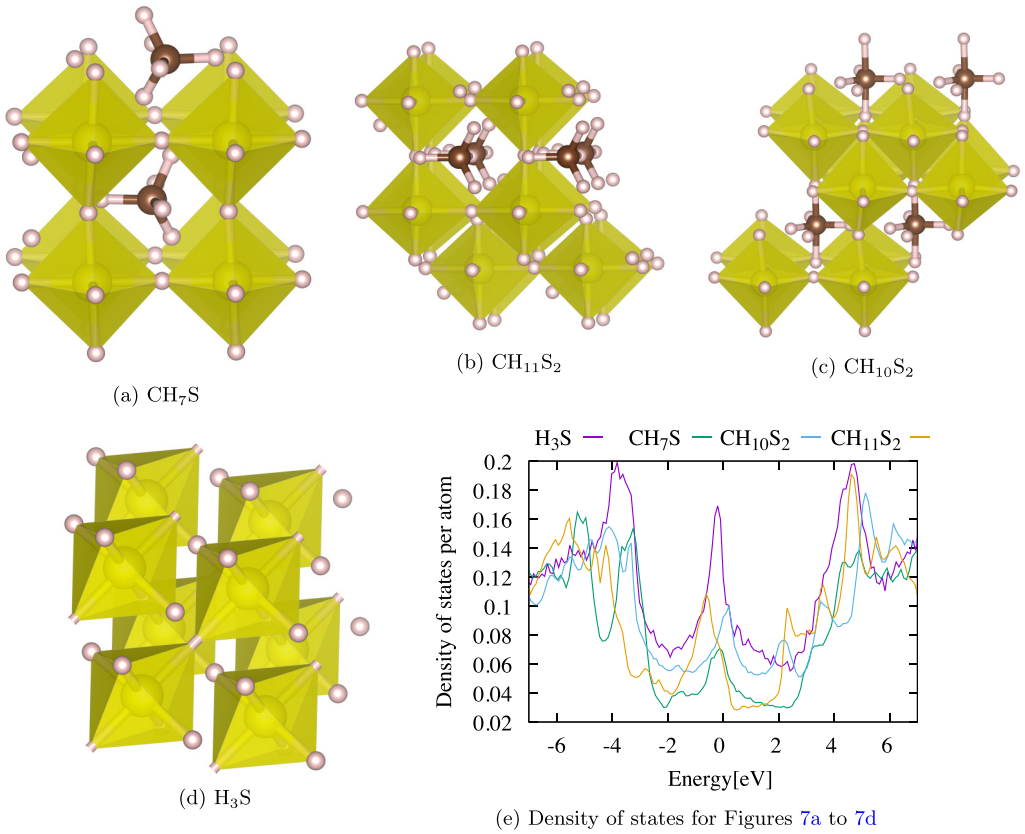

(a) CH_7S (b) $CH_{11}S_2$ (c) $CH_{10}S_2$

(d) H_3S (e) Density of states for Figures 7a to 7d

FIG. 6. A selection of the most promising structures with regards to their formation enthalpy and DOS at 250 GPa.

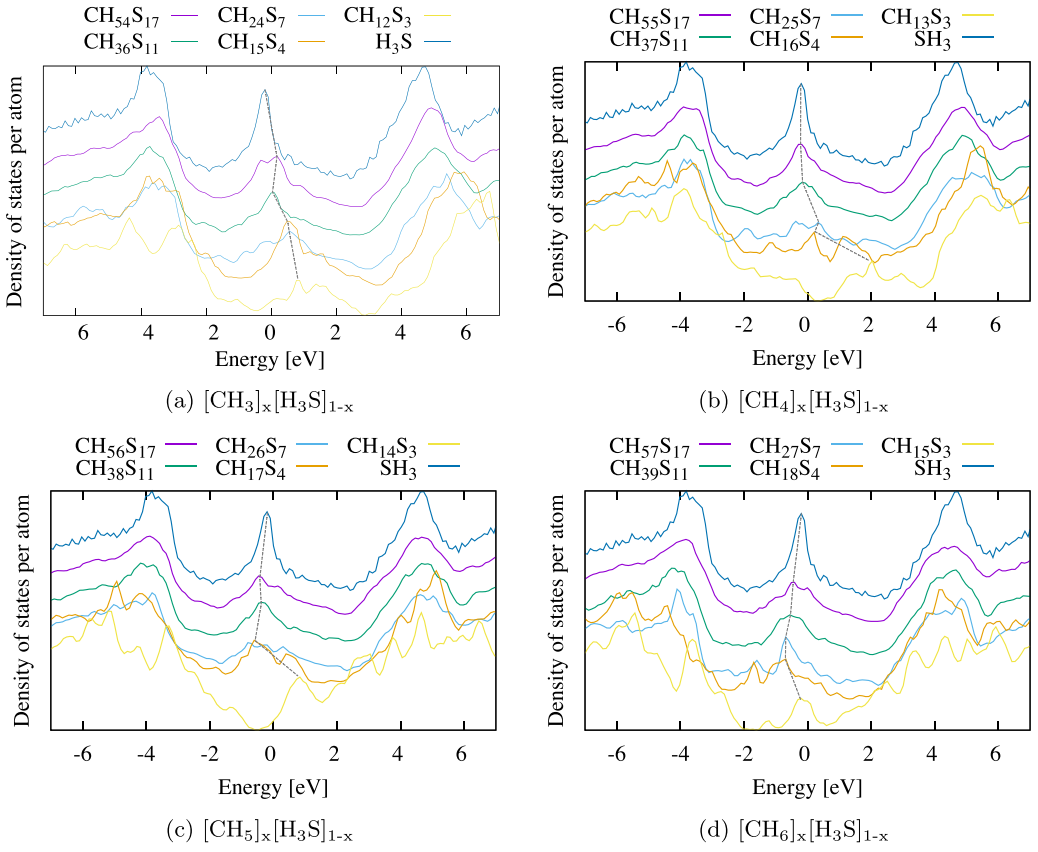

FIG. 7. Density of states in the carbon doping region at 250 GPa. The plots are normalized by the number of atoms and shifted downwards with increasing carbon doping ratio.

D. Electron phonon interaction and calculated transition temperatures

Electron phonon interactions were calculated for seven structures that have interesting peaks in the DOS at the Fermi level. Three of these systems are pictured in Fig. 6, and the rest of the structures with the corresponding DOS can be found in the GitHub repository [27].

Table I presents these selected systems and their critical temperatures. These results only confirm what the DOS analysis already indicated: The transition temperature is significantly lower than the one from H_3S at 250 GPa (203 K).

E. Structures and energies of the ternary phases at 300 GPa

Figure 8 displays the convex hull of formation enthalpy at 300 GPa. The structures assessed here generally have a higher formation enthalpy than at 250 GPa which makes them more unstable. The only stable ternary is $CH_{54}S_{17}$ with a formation enthalpy of -22 meV per atom. Apart from a slight compression of the simulated cell, the $CH_{54}S_{17}$ structure is almost identical to the one at 250 GPa. H_3S, which is the most stable structure at 250 GPa, remains the most stable system at the higher pressure. In contrast to most other systems at 300 GPa its formation enthalpy per atom even drops from -130 meV per atom to -140 meV per atom while the structure remains unchanged. Some structures with a low formation enthalpy at 250 GPa had some kind of H_3S layers in it. An example of such structures can be seen in Fig. 6. At 300 GPa those H_3S layers were still found but other, less symmetric structures have a lower enthalpy at 300 GPa.

The DOS was also calculated and analyzed for all the structures at 300 GPa. No interesting peaks at the Fermi level were found.

TABLE I. Simulated electron-phonon parameters for seven systems with interesting features in the DOS at the Fermi level. N_F is the density of states on the Fermi surface, λ the electron-phonon coupling parameter, and T_c the critical temperature in degrees Kelvin calculated according to the Allen-Dynes equation with $\mu^* = 0.1$.

	H_3S	$CH_{10}S_2$	$CH_{11}S_2$	$CH_{13}S_2$	$CH_{14}S_2$	CH_7S	CHS	CH_4S_2
N_F (eV Å^3 sp.)$^{-1}$	0.021	0.016	0.009	0.011	0.014	0.011	0.015	0.014
$\omega_{\log}$ (K)	1570	1470	1650	1045	580	1530	565	405
λ	1.5	1.17	0.64	1.05	1.77	0.92	0.89	1.24
T_c (K)	180	125	45	80	75	90	30	40

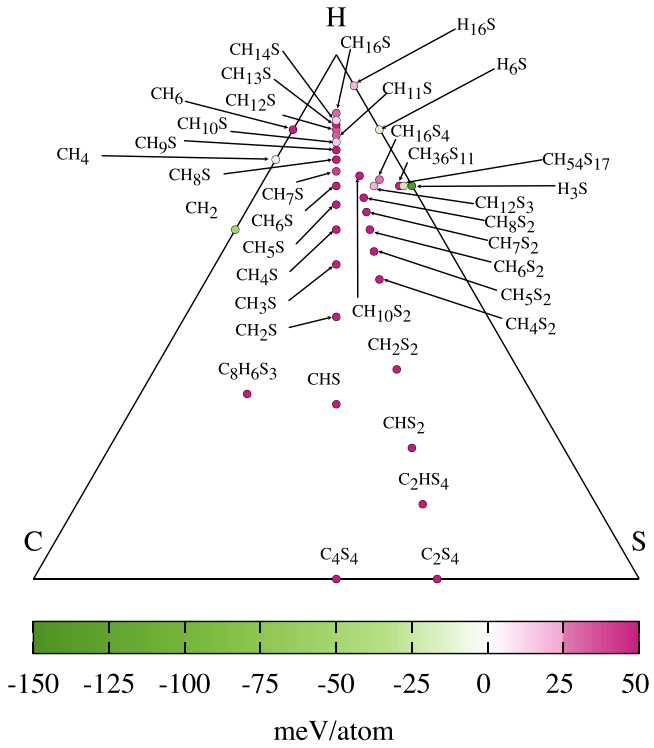

FIG. 8. The ternary convex hull of formation enthalpy at 300 GPa.

IV. CONCLUSIONS

Our extensive structure search, that sampled the ternary phase diagram densely, revealed only a small number of systems with promising peaks in the DOS, a necessary condition for conventional superconductors with high T_c [20–23]. Most of them were found in the carbon-doped H_3S region displayed in Figs. 1 and 4 and are less distinct with increased carbon content. This indicates that a higher carbon ratio in carbon-doped H_3S crystals lowers the T_c. Wang *et al.* [5] studied this carbon doping region as well and calculated the critical temperatures. Their results agree with the ones from our DOS analysis. Structures with interesting electronic DOS that are not carbon-doped H_3S crystals were further processed and the critical temperature was calculated. No structure has an exceptionally high T_c. The values can be found in Table I.

The lack of HTC superconductors for all compositions and at both pressures poses more questions than it answers. In the lack of further experimental evidence, we see the following possibilities:

The right stoichiometry of the superconductor was investigated in this and previous work, but the lowest enthalpy structure was not found. At this stage and based on our effort and the results of previous independent searches it is unlikely that the correct crystal structure was simply overlooked.

Another possibility is that the structure lies in a part of the ternary phase diagram that was not explored. However, this also seems unlikely, considering our structure search covers most of the relevant regions of the phase diagram.

So it could be that Snider *et al.* have observed an unconventional room-temperature superconductor or another phenomenon with electrical resistance drops. In that case, all of the structures with sufficiently low formation enthalpy could be candidates for the RTS structure.

Last but not least there is the possibility of an error in the experimental setup of the initial discovery. Recent publications [28,29] have actually questioned the correctness of the originally published results. Our data and the fact that no independent group has yet been able to reproduce the experiment support this option.

A selection of the 3000 best structures and their density of states is available at this GitHub repository [27]. The atomic positions and the lattice constants were relaxed using the tier 2 basis of FHI-AIMS and a tight convergence criterion of 10^{-2} eV/Å.

ACKNOWLEDGMENTS

The calculations were performed on the computational resources of the Swiss National Supercomputer (CSCS) under project s963 and on the sciCORE [30] scientific computing center at University of Basel.

[1] E. Snider, N. Dasenbrock-Gammon, R. McBride, M. Debessai, H. Vindana, K. Vencatasamy, K. V. Lawler, A. Salamat, and R. P. Dias, Room-temperature superconductivity in a carbonaceous sulfur hydride, Nature (London) **586**, 373 (2020).

[2] A. Lamichhane, R. Kumar, M. Ahart, N. P. Salke, N. Dasenbrock-Gammon, E. Snider, Y. Meng, B. Lavina, S. Chariton, V. B. Prakapenka, M. Somayazulu, R. P. Dias, and R. J. Hemley, X-ray diffraction and equation of state of the C-S-H room-temperature superconductor, J. Chem. Phys. **155**, 114703 (2021).

[3] Y. Sun, Y. Tian, B. Jiang, X. Li, H. Li, T. Iitaka, X. Zhong, and Y. Xie, Computational discovery of a dynamically stable cubic SH_3-like high-temperature superconductor at 100 GPa via CH_4 intercalation, Phys. Rev. B **101**, 174102 (2020).

[4] W. Cui, T. Bi, J. Shi, Y. Li, H. Liu, E. Zurek, and R. J. Hemley, Route to high-T_c superconductivity via CH_4-intercalated H_3S hydride perovskites, Phys. Rev. B **101**, 134504 (2020).

[5] T. Wang, M. Hirayama, T. Nomoto, T. Koretsune, R. Arita, and J. A. Flores-Livas, Absence of conventional room-temperature superconductivity at high pressure in carbon-doped H_3S, Phys. Rev. B **104**, 064510 (2021).

[6] J. E. Hirsch and F. Marsiglio, Unusual width of the superconducting transition in a hydride, Nature **596**, E9 (2021).

[7] J. E. Hirsch and F. Marsiglio, Absence of magnetic evidence for superconductivity in hydrides under high pressure, Physica C: Supercond. Appl. **584**, 1353866 (2021).

[8] J. E. Hirsch and F. Marsiglio, Nonstandard superconductivity or no superconductivity in hydrides under high pressure, Phys. Rev. B **103**, 134505 (2021).

[9] E. F. Talantsev, The electron-phonon coupling constant, fermi temperature and unconventional superconductivity in the

carbonaceous sulfur hydride 190 K superconductor, Supercond. Sci. Technol. **34**, 034001 (2021).

[10] M. Dogan and M. L. Cohen, Anomalous behavior in high-pressure carbonaceous sulfur hydride, Physica C: Supercond. Appl. **583**, 1353851 (2021).

[11] S. Goedecker, Minima hopping: An efficient search method for the global minimum of the potential energy surface of complex molecular systems, J. Chem. Phys. **120**, 9911 (2004).

[12] M. Amsler and S. Goedecker, Crystal structure prediction using the minima hopping method, J. Chem. Phys. **133**, 224104 (2010).

[13] M. Sicher, S. Mohr, and S. Goedecker, Efficient moves for global geometry optimization methods and their application to binary systems, J. Chem. Phys. **134**, 044106 (2011).

[14] S. Roy, S. Goedecker, and V. Hellmann, Bell-Evans-Polanyi principle for molecular dynamics trajectories and its implications for global optimization, Phys. Rev. E **77**, 056707 (2008).

[15] P. Salamon, P. Sibani, and R. Frost, *Facts, Conjectures, and Improvements for Simulated Annealing*, SIAM Monographs on Mathematical Modeling and Computation (Society for Industrial and Applied Mathematics, Philadelphia, 2002).

[16] D. J. Wales and J. P. K. Doye, Global optimization by basin-hopping and the lowest energy structures of Lennard-Jones clusters containing up to 110 atoms, J. Phys. Chem. A **101**, 5111 (1997).

[17] A. Kozhevnikov, M. Taillefumier, and S. Pintarelli, SIRIUS, https://github.com/electronic-structure/SIRIUS (2021).

[18] A. Dal Corso, Pseudopotentials periodic table: From H to Pu, Comput. Mater. Sci. **95**, 337 (2014).

[19] J. P. Perdew, K. Burke, and M. Ernzerhof, Generalized Gradient Approximation Made Simple, Phys. Rev. Lett. **77**, 3865 (1996); Generalized Gradient Approximation Made Simple [Phys. Rev. Lett. **77**, 3865 (1996)] **78**, 1396(E) (1997).

[20] J. A. Flores-Livas, L. Boeri, A. Sanna, G. Profeta, R. Arita, and M. Eremets, A perspective on conventional high-temperature superconductors at high pressure: Methods and materials, Phys. Rep. **856**, 1 (2020).

[21] I. Errea, M. Calandra, C. Pickard, J. Nelson, R. Needs, Y. Li, H. Liu, Y. Zhang, Y. ma, and F. Mauri, Quantum hydrogen-bond symmetrization in the superconducting hydrogen sulfide system, Nature (London) **532**, 81 (2016).

[22] I. Errea, F. Belli, L. Monacelli, A. Sanna, T. Koretsune, T. Tadano, R. Bianco, M. Calandra, R. Arita, F. Mauri, and J. Flores-Livas, Quantum crystal structure in the 250-Kelvin superconducting lanthanum hydride, Nature (London) **578**, 66 (2020).

[23] X. Zhang, Y. Zhao, and G. Yang, Superconducting ternary hydrides under high pressure, WIREs Comput Mol. Sci., e1582 (2021).

[24] P. Giannozzi, S. Baroni, N. Bonini, M. Calandra, R. Car, C. Cavazzoni, D. Ceresoli, G. L. Chiarotti, M. Cococcioni, I. Dabo, A. D. Corso, S. de Gironcoli, S. Fabris, G. Fratesi, R. Gebauer, U. Gerstmann, C. Gougoussis, A. Kokalj, M. Lazzeri, L. Martin-Samos *et al.*, QUANTUM ESPRESSO: A modular and open-source software project for quantum simulations of materials, J. Phys.: Condens. Matter **21**, 395502 (2009).

[25] P. B. Allen and R. C. Dynes, Transition temperature of strong-coupled superconductors reanalyzed, Phys. Rev. B **12**, 905 (1975).

[26] J. Flores-Livas, M. Graužinytė, L. Boeri, G. Profeta, and A. Sanna, Superconductivity in doped polyethylene at high pressure, Eur. Phys. J. B **91**, 176 (2018).

[27] https://github.com/moritzgubler/C-H-S_250GPa.

[28] J. E. Hirsch, Faulty evidence for superconductivity in ac magnetic susceptibility of sulfur hydride under pressure, arXiv:2109.08517.

[29] R. F. Service, Breakthrough or bust? Claim of room-temperature superconductivity draws fire, Science **374**, 520 (2021).

[30] http://scicore.unibas.ch/.